Photocrosslinking of polyacrylamides using [2+2] photodimerisation of monothiomaleimides

Mohammed Aljuaid,[a,b] Hannes A. Houck , [a,c] Spyridon Efstathiou,[a] David M. Haddleton [a*] Paul Wilson [a*]

[a] *Department of Chemistry, University of Warwick, Library Road, CV4 7AL, Coventry, UK.*

[b] *Department of Chemistry, Turabah University College, Taif University, P.O. Box 11099, Taif 21944, Saudi Arabia.*

[c] *Institute of Advanced Study, University of Warwick, CV4 7AL, Coventry, UK.*

E-mail: p.wilson.1@warwick.ac.uk; d.m.haddleton@warwick.ac.uk

For Table of Contents use only

Abstract

The [2+2] photocycloaddition of monothiomaleimides (**MTM**) has been exploited for the photocrosslinking of polyacrylamides. Polymer scaffolds composed of dimethylacrylamide (DMA) and varying amounts of D,L-homocysteine thiolactone acrylamide (5, 10, and 20 mol%) were synthesised *via* free radical polymerisation (FRP), whereby the latent thiol-functionality was exploited to incorporate **MTM** motifs. Subsequent exposure to UV light (λ = 365 nm, 15 mW cm^{-2}) triggered intermolecular crosslinking *via* the photodimerisation of **MTM** side chains, thus resulting in the formation of polyacrylamide gels. The polymer scaffolds were characterised using Fourier transform infrared spectroscopy (FT-IR), UV-Visible spectroscopy (UV-Vis), ^{1}H NMR, and size exclusion chromatography (SEC), confirming the occurrence of the [2+2] photocycloaddition between the **MTM** moieties. The mechanical and physical

properties of the resulting gels containing various **MTM** mol% were evaluated by rheology, compression testing, and swelling experiments. In addition, scanning electron microscopy (SEM) was used to characterise the xerogel morphology of 5 and 10 mol% **MTM** hydro- and organo-gels. The macro-porous morphology obtained for the hydrogels was attributed to phase separation due to the difference in solubility of the PDMA modified with thiolactone side chains, provided that a more homogeneous morphology was obtained when the photo-gels were prepared in DMF as the solvent.

Introduction

Polymer scaffolds have proven to be useful materials for several applications, including tissue engineering,[1] drug delivery,[2] biosensors,[3] as well as filtration membranes in separation processes for gaseous and liquid mixtures.[4] These materials can be synthesised using several conjugation reactions, such as Diels-Alder,[5-8] thiol-ene,[9-12] and [2+2] photocycloaddition.[13-17] Maleimides have been shown to be excellent candidates for these conjugation reactions due to its electrophilic characteristic that is attributed to the relatively low energy $\pi_{C=C}$* orbital. However, the [2+2] photocycloaddition of maleimides, in batch, is relatively slow, requiring long irradiation times and high energy UV-light (270-320 nm), which is not always desirable especially for sensitive substrates such as biomolecules.[18] Nonetheless, there have been several reports demonstrating the use of [2+2] photodimerisation of maleimides for the formation of covalent crosslinked networks. For example, polymethacrylates bearing maleimide groups have been photochemically crosslinked under UV irradiation without the need for a photosensitiser,[19] although a two-fold increase in crosslinking rate occurred when thioxanthone was added. Another report introduced the photocrosslinking of both co- and ter-polyacrylamide co-polymers using 2-(dimethylmaleimido)-*N*-ethyl acrylamide as the

photoactive comonomer, in order to obtain pH and temperature responsive hydrogels.[20] It is noteworthy that incomplete curing of the maleimide side chain groups is typically achieved, although this can be exploited for further functionalisation using Diels-Alder or thiol-ene reactions.[21-22] This allows for the introduction of more complexity and functionality into the formed materials, for instance by covalently attaching biomolecules to the scaffold using thiol-maleimide Michael addition. A two-photon induced curing of maleimides using near-IR irradiation (λ = 800 nm) has also been developed, giving access to highly resolved [2+2]-crosslinked 3D microfabricated networks.[23] Hence, an alternative [2+2]-crosslinking strategy for maleimide-based formulations at much longer wavelengths and lower energy became available, enabling a more benign route for hydrogel formation under physiological conditions.

Recently, monothiomaleimide (**MTM**) has been reported as an efficient and highly specific reagent towards [2+2] photocycloaddition (Figure 1a).[24] The substitution on the maleimide ring by a thiol group was shown to red-shift the wavelength of maximum absorption from 270 up to 339 nm. Moreover, **MTMs** have been demonstrated to undergo highly efficient and stereoselective (*exo*, head-to-head) [2+2] photodimerisation within 5 minutes, including in water-acetonitrile mixtures (e.g. 95:5 v/v) at concentrations as low as 72 µM. This led to **MTMs** being excellent candidates for photochemically rebridging the disulfide bond in biomolecules (Figure 1b).[25] Only recently, the potential of [2+2] photodimerisation of **MTMs** was explored in polymer conjugation reactions, as illustrated by the quantitative coupling of linear and brush-like **MTM** end-capped hydrophilic polymers in only 10 minutes.[26]

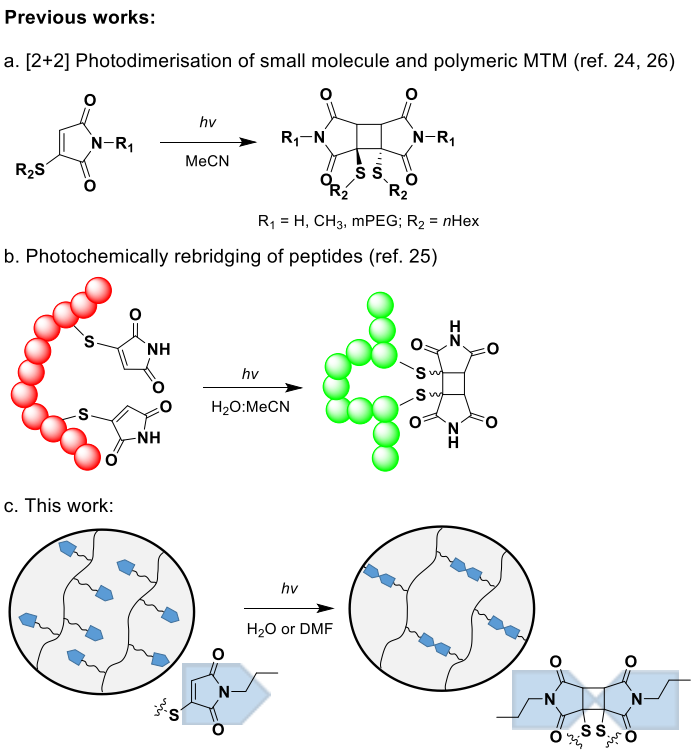

Fig 1. a) Previous works on the [2+2] photocycloaddition of **MTM** for small molecule and polymer conjugation, b) photochemical re-bridging of MTM-modified biomolecules, and c) exploitation of the **MTM**-[2+2] photocrosslinking for hydro- and organogel formation.

Herein, we further extend the scope of the thiomaleimide [2+2] photodimerisation reaction into polymer chemistry by reporting, for the first time, the synthesis of **MTM** side chain functionalised polymers and their subsequent photo-crosslinking under irradiation (Figure 1c).

Results and discussion

In order to attach **MTM** into the polymer chain, the chosen strategy was to copolymerise dimethyl acrylamide (**DMA**) and D,L-homocysteine thiolactone acrylamide monomer (**TLA**) *via* FRP (**Scheme 1A**). The resulting **TLA**-containing polymer precursor hence provided an alternative route for the incorporation of the **MTM** motifs into the polymer scaffolds via a straightforward post-polymerisation reaction. This strategy was devised since direct use of an **MTM**-acrylamide monomer was expected to result in side-reactions during its FRP, which is commonly observed for pendant maleimide motifs. As previously reported, TLA readily

undergoes ring opening *via* aminolysis, thereby liberating a free sulfhydryl group that becomes available for further functionalisation (Scheme 1B).[27] In our approach, these free sulfhydryls were used to react with *N*-propyl monobromomaleimide (**MBM**) *via* an addition-elimination mechanism, to obtain the **MTM**-functionalised polymer scaffolds (**Scheme 1C**). In a final step, the **MTM** based polymer solutions were exposed to UV light (365 nm, 15 mW cm^{-2}), leading to the [2+2] photodimerization of **MTM** moieties and thus crosslinking of the polymer (**Scheme 1D**).

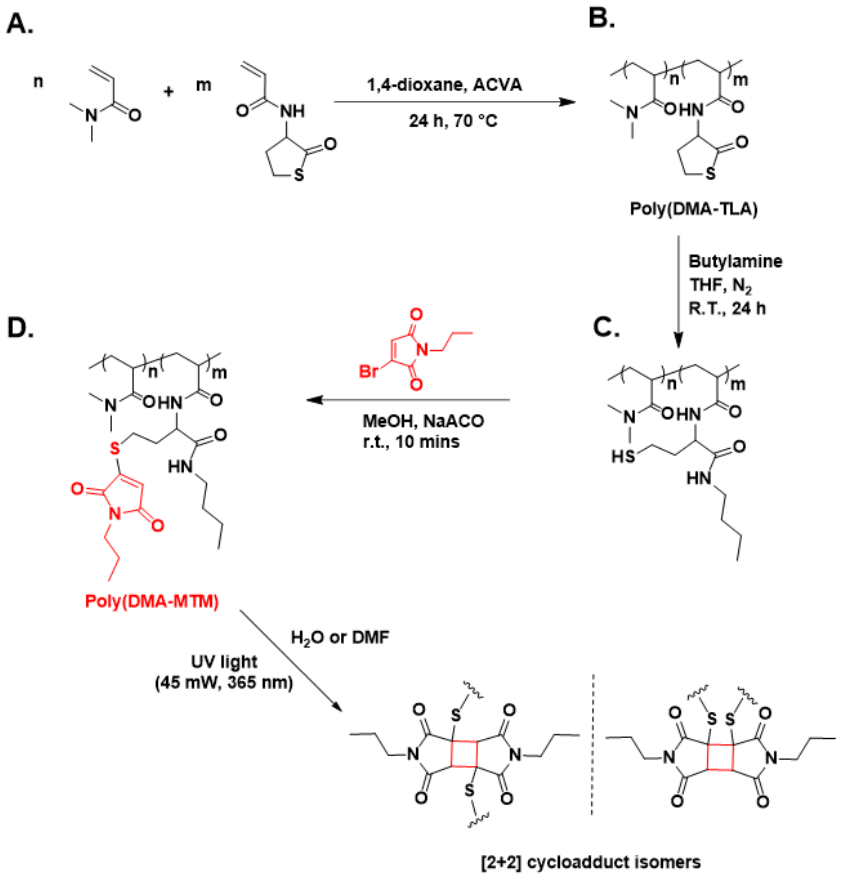

Scheme 1. Schematic representation of the devised synthesis strategy towards **poly(DMA-MTM)** scaffolds. **A**) Free radical copolymerisation of **DMA** and **TLA**, followed by **B**) aminolysis of the side chains resulting in homocysteine thiolactone ring opening and the liberation of thiol functionalities. **C**) Thiol-bromo post-modification reaction with **MBM** eventually gives the **MTM** functionalised polymers, **D**) which can self-crosslink under UV irradiation *via* a [2+2] dimerisation (365 nm, 15 mW cm^{-2}).

The synthesis of **TLA** monomer was achieved by the addition of acryloyl chloride to D,L-homocysteine thiolactone hydrochloride according to a literature procedure.[28] The monomer

was characterised by ^{1}H and ^{13}C NMR (**Fig. S1, ESI**) with the most important finding for the **TLA** monomer characterisation being the presence of the olefin group at 5.65 and 6.18 ppm, thus indicated the successful synthesis of the monomer. Additionally, the N-H peak of the amide group was observed at 8.46 ppm, which confirmed the formation of the acrylamide monomer. The integration of all proton signals agreed with the chemical structure of the monomer.

The synthesis of **MBM** compound was achieved by reacting propylamine with bromomaleic anhydride. ^{1}H and ^{13}C NMR spectroscopy confirmed the chemical structure of **MBM** (**Fig. S2, ESI**). Indeed, the methylene peak directly linked to the imide group was detected at 3.45 ppm and its integration with the olefin peak at 6.8 ppm was found to be 2:1, respectively. Electron-spray-ionisation mass spectroscopy (ESI-MS) confirmed the molecular weight of **MBM**, and the presence of bromine atom isotopic distribution was evident. This finding was important to ensure the **MBM** compound could participate in the addition-elimination reaction with the latent sulfhydryl groups from the polymer scaffolds.

The **TLA** monomer was copolymerised with **DMA**, which was selected as a hydrophilic acrylamide monomer. Three co-polymers were synthesised by FRP in 1,4-dioxane using 4,4'-azobis(4-cyanovaleric acid) (ACVA) as an initiator with different co-monomer composition through changing the relative mole fraction of **DMA** and **TLA** (Table 1). The polymerisation was performed at 70 °C and left overnight with monomer conversion determined by ^{1}H NMR. The **TLA** content was calculated by integrating the dimethyl peak of **DMA** (2.65-3.09 ppm) and the C-H of **TLA** (4.55 ppm) (**Fig. 2A**). Table 1 summarises the experimentally observed **TLA** composition and the molecular weight data and dispersity obtained from SEC measurements of the prepared copolymers (**Fig. S4**).

Table 1. Characterisation of the synthesised poly(DMA-TLA) co-polymers.

Entry	TLA %[a]	$M_{w,SEC}$ (g.mol^{-1})[b]	$M_{n,SEC}$ (g.mol^{-1})[b]	$Đ$
Poly(DMA-TLA)$_{5\%}$	5.3	62,400	22,100	2.82
Poly(DMA-TLA)$_{10\%}$	9.8	64,200	19,200	3.33
Poly(DMA-TLA)$_{20\%}$	25	62,100	21,400	2.89

[a]**TLA** % was calculated by the integration ratio between **DMA** (δ = 2.65-3.09 ppm) and the CH of **TLA** peak (δ = 4.55 ppm).
[b]Determined from SEC analysis using narrow PMMA standards.

Subsequently, the thiolactone moieties were ring-opened through aminolysis with butyl amine in order to release the latent thiol functionality (**Fig. 2**, S3, and S5). The proton resonances corresponding to the **TLA** could be used to evaluate the ring-opening step, as the signal of CH from thiolactone ring would be shifted from 4.55 ppm to 4.27 ppm. Additionally, the methyl group from butylamine was observed at 0.87 ppm. Eventually, **MBM** was introduced to react with the liberated sulfhydryl functionalities which resulted in the formation of **poly(DMA-MTM)s** bearing thiomaleimide groups in the polymer side chains (Fig. 2, Fig. S7). The successful incorporation of **MTM** in the polymer scaffolds was confirmed by ^{1}H NMR, as the olefin proton appeared at 6.60 ppm. The sulfhydryl degree of modification was calculated from the ratio of C-H peak at 4.27 ppm and the olefin peak at 6.60 ppm, and was found to be 90%, 95%, and 75% for **poly(DMA-TLA)$_{5\%}$**, **poly(DMA-TLA)$_{10\%}$**, and **poly(DMA-TLA)$_{20\%}$**, respectively. It is possible that some disulfide bond formation occurred during the aminolysis process, explaining why the sulfhydryls did not reach full conversion to **MTMs**.

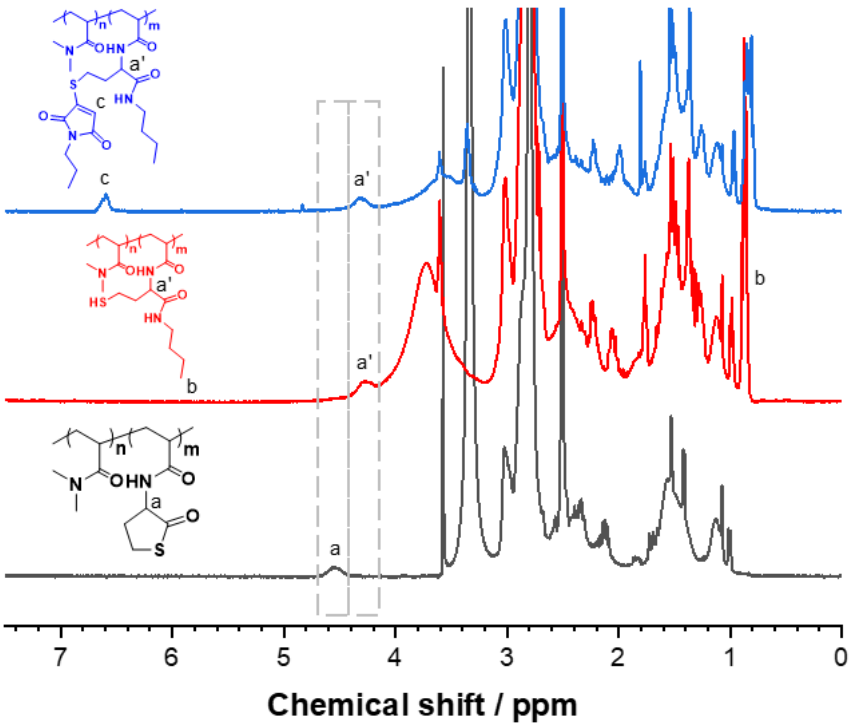

Fig 2. ^{1}H NMR spectra of **poly(DMA-TLA)$_{10\%}$** (black, bottom), the ring-opened **poly(DMA-TLA)$_{10\%}$** (red, middle), and **poly(DMA-MTM)$_{10\%}$** (blue, top).

The sequential polymer modification steps were additionally analysed by FT-IR spectroscopy to further evidence the thiolactone ring opening and the formation of sulfhydryl groups, as observed by the significant reduction of the peak at 1705 cm^{-1} after the aminolysis step. The covalent attachment of **MTM** onto the polymer was also confirmed by FT-IR spectroscopy, with an increase in the peak at 1705 cm^{-1} attributed to the introduction of the imide group from **MTM** (**Fig. 3**, Fig. S9, S10).

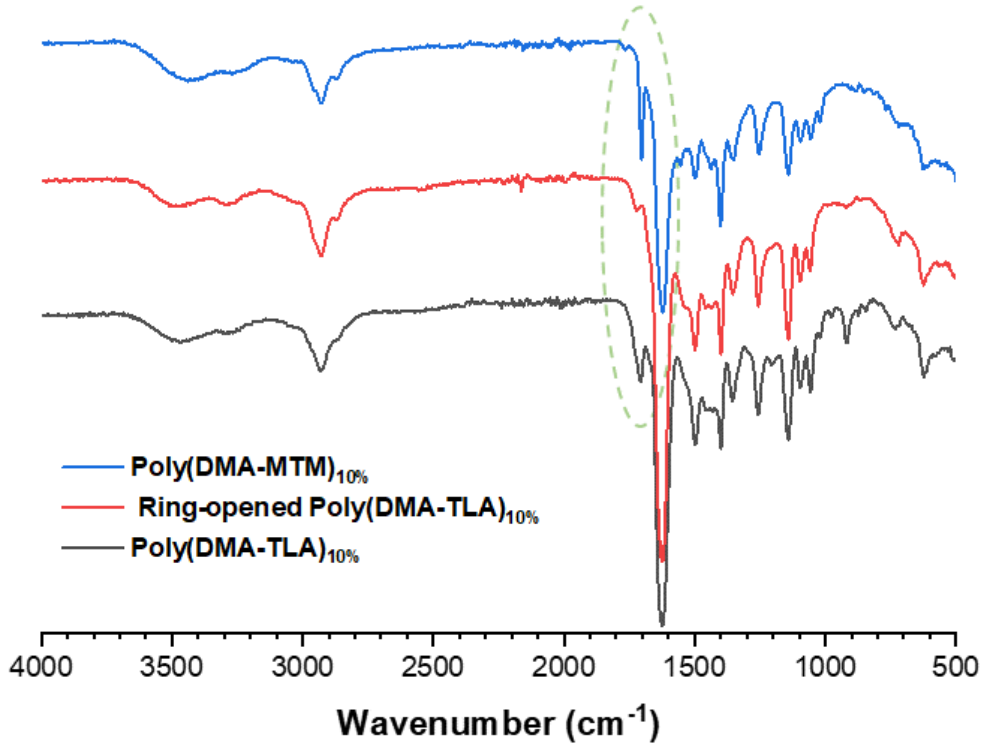

Fig 3. FT-IR spectroscopy of **poly(DMA-TLA)$_{10\%}$** (black, bottom), the ring-opened **poly(DMA-TLA)$_{10\%}$** (red, middle), and **poly(DMA-MTM)$_{10\%}$** (blue, top).

Besides NMR and IR spectroscopy, also SEC analysis was performed to monitor the polymer modification steps *via* the traces arising from the refractive index (RI, Fig. S6, S8)) and UV detectors. The UV detector was set at λ = 365 nm, selected based on the absorption spectra of the **poly(DMA-MTM)** scaffolds (**Fig. S11B, S11D, and S11F**) which exhibited little absorbance above 360 nm prior to reaction with **MBM**. Pleasingly, the traces from the RI and UV coincided, thereby confirming the covalent attachment of **MTMs** to the polymer and thus that the targeted scaffolds had been successfully synthesised (**Fig. S11A, S11C, and S11E**).

With the **MTM**-functionalised polymer scaffolds in hand, their potential to undergo photocrosslinking to yield polyacrylamide gels was next explored. At first, the photoreactivity of the **MTM**-containing polymers was investigated. For this, UV-Vis spectroscopy was used to monitor the chemical changes occurring during the UV irradiation. The absorbance peak for MTM, at 360 nm, significantly reduced after only 2 minutes, and continued to reduce in

intensity until complete consumption was observed after 20 minutes (**Fig. 4**). This experiment was conducted as additional prove of the occurrence of the **MTM**-[2+2] photocycloaddition being responsible for the photo-gelation.

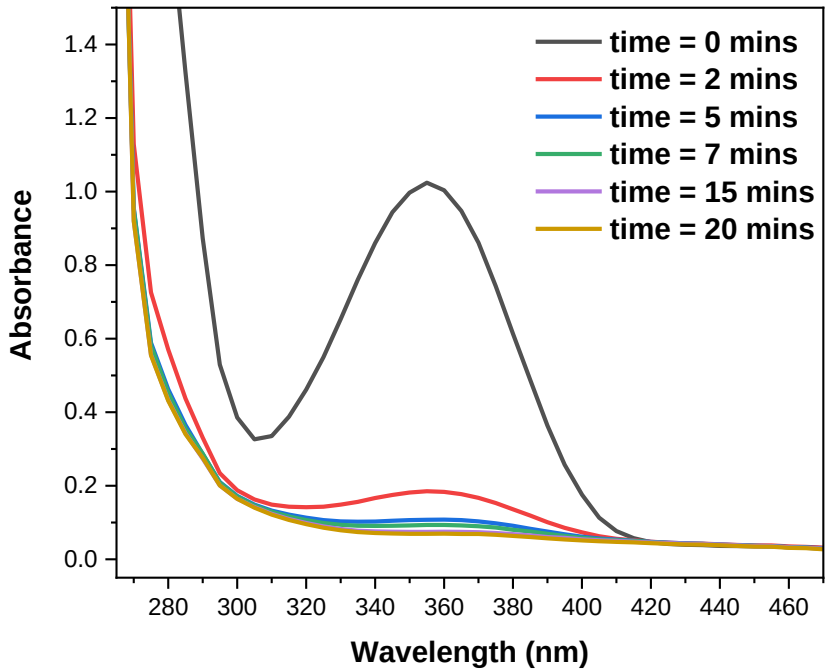

Fig 4. UV-vis spectroscopy monitoring the consumption of **MTMs** (λ = 360 nm) during the irradiation of **poly(DMA-MTM)$_{10\%}$** solution using a 365 nm Lumidox II 96-Position LED array set at 45 mW (15 mW cm^{-2}).

Besides UV-Vis monitoring, additional experiments were performed using ^{1}H NMR spectroscopy. For this, the **poly(DMA-MTM)** polymers were dissolved in DMSO-d_6 at low concentrations (i.e. 2 wt%) and exposed to UV light (365 nm, 15 mW cm^{-2}) in order to follow the chemical changes of the **MTM** moieties under irradiation. Although these reaction conditions did not lead to gelation, valuable information about the reaction kinetics of the macromolecular substrates was obtained. The olefin peak at 6.60 ppm was monitored by ^{1}H NMR over time during UV exposure, which decreased during the irradiation time until it was fully consumed within 45 minutes (**Fig. 5A, 5B, and 5C**). Plotting the conversion against the irradiation time revealed that the consumption of the **MTM** was of the order **poly(DMA-MTM)$_{5\%}$** > **poly(DMA-MTM)$_{10\%}$** > **poly(DMA-MTM)$_{20\%}$**, with **poly(DMA-MTM)$_{5\%}$** reaching 100% conversion after 30 minutes whilst **poly(DMA-MTM)$_{10\%}$** and **poly(DMA-MTM)$_{20\%}$**

reached 85% and 80%, respectively. However, both **poly(DMA-MTM)$_{10\%}$** and **poly(DMA-MTM)$_{20\%}$** reached near-quantitative conversion after 45 minutes of UV irradiation (**Fig. 5D**).

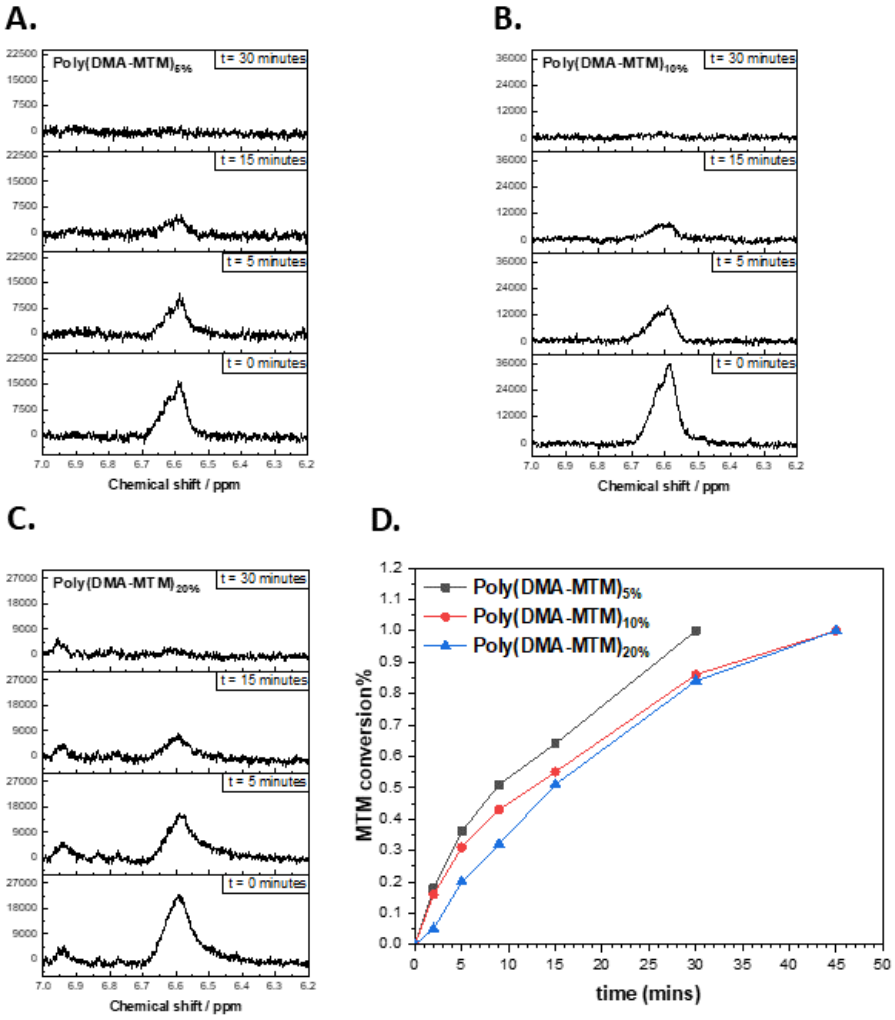

Fig 5. The olefinic peak followed during the irradiation for A) (**poly(DMA-MTM)$_{5\%}$**, B) (**poly(DMA-MTM)$_{10\%}$**, and C) **(poly(DMA-MTM)$_{20\%}$**, ;D) kinetics of the [2+2] photodimerisation of **MTM** within the polymers; y-axis represents the following olefinic peak collected by ^{1}H NMR in DMSO-d_6 and x-axis represents the irradiation time.

Having confirmed the photoreactivity of the **MTM** moieties, the **poly(DMA-MTM)** substrates were then dispersed in aqueous media to examine their photo-crosslinking for the formation of hydrogels. While the 5 and 10% functionalised PDMA polymers remained water soluble, polymers containing 20% of **MTM** were insoluble in water. Consequently, for the purposes of gelation, the solvent was changed to DMF, which was shown to be a good solvent for all the scaffolds under investigation. Different concentrations were tested in order to select the

appropriate condition for gelation. It was observed that 20 wt% of **poly(DMA-MTM)$_{20\%}$** was the solubility limit, therefore this concentration was chosen for all the scaffolds in order to investigate the photocrosslinking. Thus, 20 wt% of the three polymer scaffolds were dissolved in DMF and the solutions were exposed to UV light (365 nm, 15 mW cm^{-2}) for 48 hours to ensure complete conversion. Gels were qualitatively formed from each polymer solution as shown by a simple vial inversion test (**Fig. 6**). The photo-gels were then dried in a vacuum oven in order to remove the DMF solvent and then characterised using FT-IR spectroscopy. The aim for IR characterisation was to assess whether photocrosslinking indeed occurred due to [2+2] photodimerisation of the **MTM**. This was confirmed as the imide group from the thiomaleimide ring is expected to have a lower wavenumber due to the conjugation between the imide and C=C, which is lost upon the formation of the succinimide cycloadducts after the photodimerisation, thus leading to a small increase in the imide wavenumber. FT-IR revealed that the imide group of the uncured polymer appeared at 1702 cm^{-1}, but shifted to 1712 cm^{-1} after the gelation (**Fig. S13, ESI**).

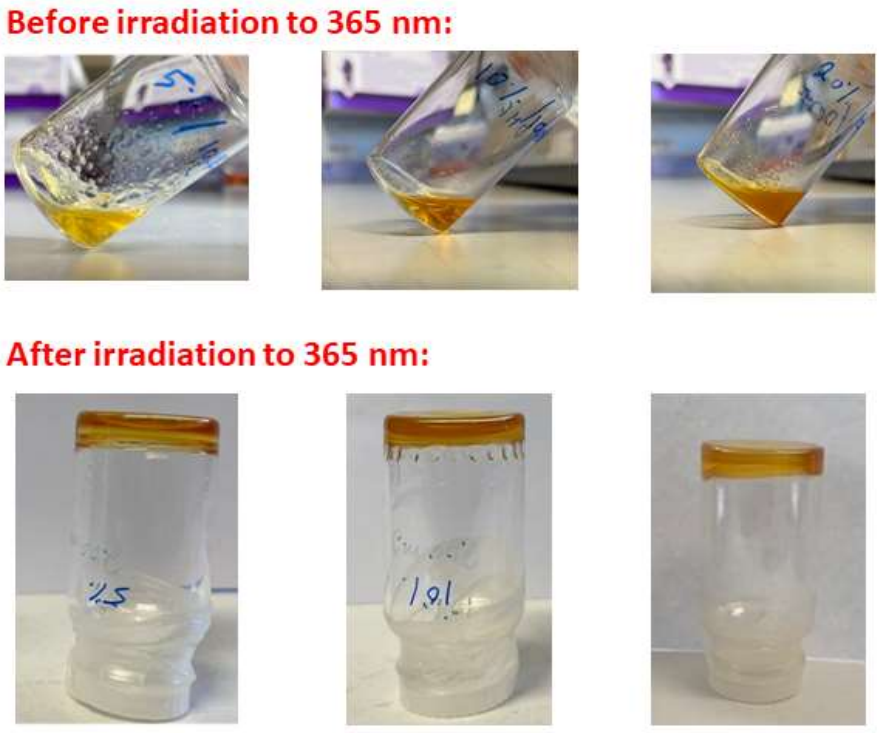

Fig 6. Pictures of the **poly(DMA-MTM)$_{5\%}$ (left), poly(DMA-MTM)$_{10\%}$ (middle), and poly(DMA-MTM)$_{20\%}$ (right)** gels before (top) and after (bottom) 48 hours of UV irradiation (365 nm, 15 mW cm^{-2}) in DMF.

With successful photo-crosslinking demonstrated, the viscoelastic properties of the photo-cured gels were evaluated by oscillatory shear mode rheology at 25 °C allowing for their storage (G') and loss (G'') moduli to be determined. Amplitude sweep experiments at a constant frequency of 10 rad.s^{-1} were carried out on all samples to confirm all measurements were conducted within the linear viscoelastic regime (**Fig. 7A**). The G' value of the photo-gel that contained the highest amount of **MTM** moieties (i.e. **poly(DMA-MTM)$_{20\%}$**) was higher than that observed for **poly(DMA-MTM)$_{10\%}$** and **poly(DMA-MTM)$_{5\%}$**, respectively, indicative of a higher crosslinking density. The G' values for **poly(DMA-MTM)$_{5\%}$** were constant during the measurement region (1 - 100%), while **poly(DMA-MTM)$_{20\%}$ and poly(DMA-MTM)$_{10\%}$** reached a crossover point at 11% and 71% shear strains, respectively showing that a higher **MTM** content turned the materials more brittle preventing them to withstanding high shear strains along with a faster decrease in their G'. Next, frequency sweep experiments were conducted at 25 °C and at a constant strain value (γ) of 1%, selected based from the amplitude

sweeps wherein G' was fairly constant for all the photo-gels. The angular frequency was altered from 1 to 100 rad.s^{-1} (**Fig. 7B**). It was seen that the G' was constant for all the materials during the experiment regardless of the photocrosslinking density, indicating the formation of a stable covalent network. The highest G' value was found for **poly(DMA-MTM)$_{20\%}$ (4,700 Pa)**, while 945 and 3,400 Pa were found for **poly(DMA-MTM)$_{5\%}$** and **poly(DMA-MTM)$_{10\%}$**, respectively. A similar trend was observed for the G'' with 5% **MTM** showing the lowest value (27 Pa), while the 20% **MTM** had the highest G'' value (1090 Pa).

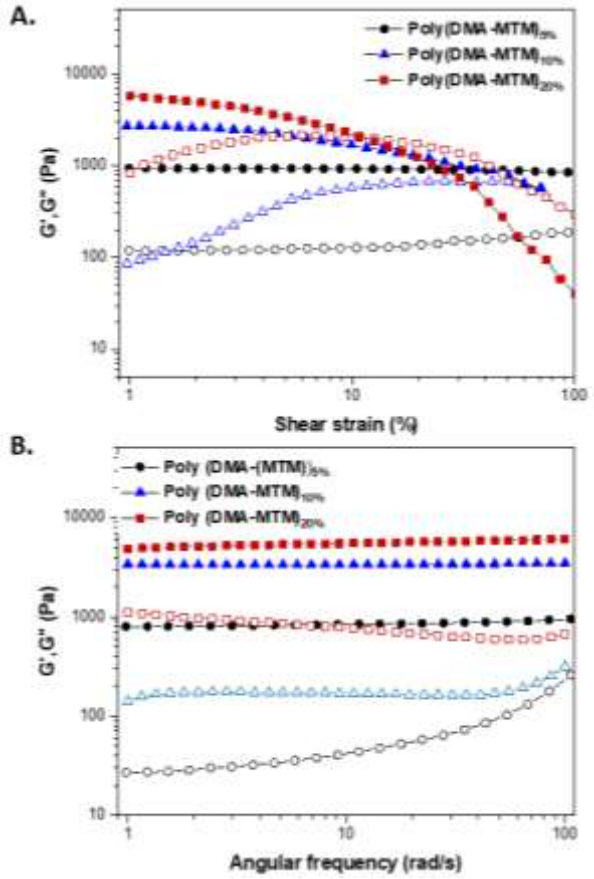

Fig 7. Amplitude sweep measurements of **poly(DMA-MTM)s** photo-gels at a constant frequency of ω = 10 rad.s^{-1} at 25 °C (A), and frequency sweep measurements of **poly(DMA-MTM)s** photo-gels using a constant strain of γ = 1 % at 25 °C (B).

Complementary to rheology investigations, compression tests were performed in order to characterise their elasticity and resistance against force. These experiments were performed since the **poly(DMA-MTM)$_{20\%}$**- and **poly(DMA-MTM)$_{10\%}$**-based gel were noticed to be very

brittle, while their **poly(DMA-MTM)$_{5\%}$** analogue seemed to be resistant against deformation and more flexible under pressure. These visual observations were confirmed by compression test measurements and revealed that higher photocrosslinking density resulted in higher stress point (**Fig. 8A**). The actual value of **poly(DMA-MTM)$_{5\%}$** stress was considerably low in comparison to the other two photo-gels (i.e. 2.9 MPa). There was no significant difference in the strain values of **poly(DMA-MTM)$_{10\%}$** and **poly(DMA-MTM)$_{20\%}$**, and they were found in between 2.5 and 3.5 %, which explained the brittle characteristics of these photo-gels. However, **poly(DMA-MTM)$_{20\%}$** was found capable to withstand more stress than **poly(DMA-MTM)$_{10\%}$** as expected (**Fig. 8A**). The brittleness of **poly(DMA-MTM)$_{10\%}$** and **poly(DMA-MTM)$_{20\%}$** could be attributed to the high photocrosslinking density and increase in the heterogeneity of the photogels, thereby restricting polymer chain extension when stress was applied.[29]

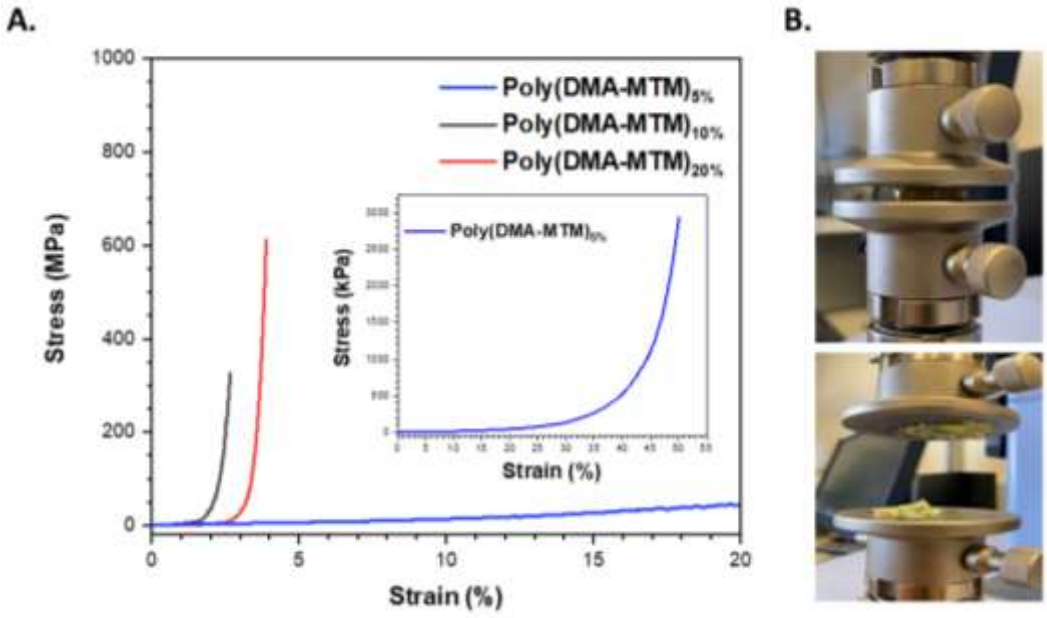

Fig 8. Compression test for **poly(DMA-MTM)$_{5\%}$**, **poly(DMA-MTM)$_{10\%}$**, and **poly(DMA-MTM)$_{20\%}$** gels (A); a photo-gel before and after the compression test experiment (B).

Finally, swelling tests were performed in water to investigate the difference in the swelling behaviour of the xerogels, obtained after vacuum drying (**Fig. 9**). Theoretically, the lower the

crosslink density, the higher the solvent amount that can be taken up by the xerogel.[30] Plotting the swelling ratio, which was calculated from equation **1**, against time revealed that **poly(DMA-MTM)$_{5\%}$** swelled more in water (12 g/g, 240 mins) compared to **poly(DMA-MTM)$_{10\%}$** (9 g/g, 240 mins) and **poly(DMA-MTM)$_{20\%}$** (5 g/g, 240 mins) due to formation of a bigger mesh size able to occupy a higher amount of water agreeing well with the low G' values. The final equilibrium swelling ratio was measured after 48 and 72 hours and found to be 15, 10, and 6 g/g for **poly(DMA-MTM)$_{5\%}$**, **poly(DMA-MTM)$_{10\%}$**, and **poly(DMA-MTM)$_{20\%}$**, respectively.

$$\textbf{Swelling ratio} = \frac{Ws - Wd}{Wd} \qquad \text{(eq. 1)}$$

Where W_d and W_s are the weights of the dried and swollen gels.

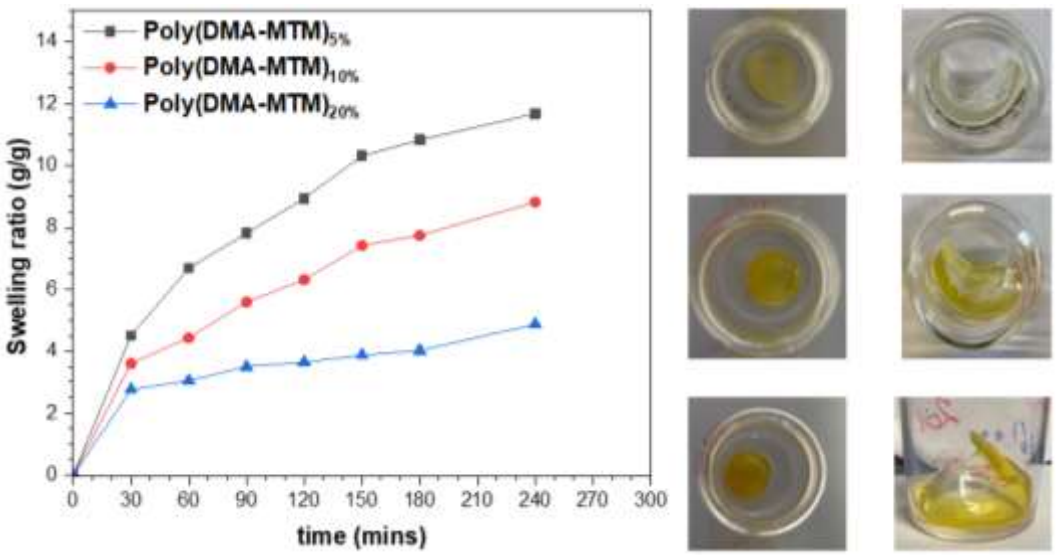

Figure 9. Swelling test for **poly(DMA-MTM)$_{5\%}$**, **poly(DMA-MTM)$_{10\%}$**, and **poly(DMA-MTM)$_{20\%}$** xerogels; y-axis represents the swelling ratio determined from the weight of the swollen and xerogel; x-axis represents the swelling period from 0 to 240 minutes.

Since **poly(DMA-MTM)$_{20\%}$** was insoluble in water leading to undesirable precipitation, (**Fig. S14, ESI**), only **poly(DMA-MTM)$_{5\%}$** and **poly(DMA-MTM)$_{10\%}$** were formulated in aqueous media and their inner structure was visualized by scanning electron microscopy (SEM). It was observed that both xerogels had porous morphologies with **poly(DMA-MTM)$_{10\%}$**

demonstrating larger pores (11.19 µm) than **poly(DMA-MTM)$_{5\%}$** (2.64 µm) (**Fig. 10**). Initially, this was surprising considering that a lower crosslinking density should result in larger mesh sizes within the network matrix. However, having previously hypothesised that increasing the mole fraction of the **MTM-**functionalised side chains reduced the water solubility of the scaffolds, in combination with the observed macro-phase separation of **poly(DMA-MTM)$_{20\%}$** during swelling in water, the increase in pore size here was likely attributed to the **MTM-**functionalised side chains arranging themselves to minimise their interactions with water, thereby leading to larger pores. In contrast, no macro-porosity was observed from the SEM images of **poly(DMA-MTM)$_{5\%}$** and **poly(DMA-MTM)$_{10\%}$** xerogels synthesized in DMF (**Fig. S15 and S16, ESI**), reinforcing this theory. In fact, the xerogels formed using DMF solvent seemed to be homogeneous with an absence of phase separation as explained by the better solubility of the polymer precursors in the organic solvent. These data indicated the presence of phase separation when water solvent was used, which could be useful for some applications that require such macro-porous networks, such as biomedical applications and tissue engineering.[31]

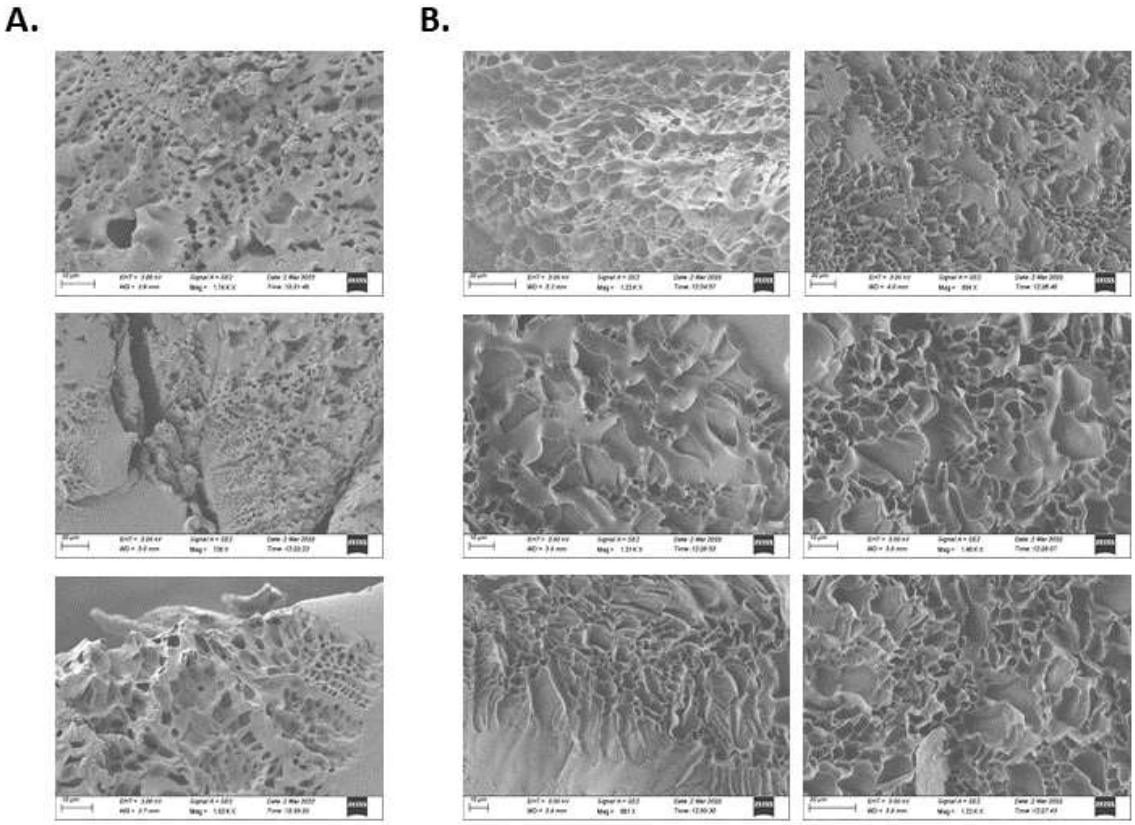

Figure 10. Scanning electron microscopy of dried **poly(DMA-MTM)$_{5\%}$** (A) and **poly(DMA-MTM)$_{10\%}$**, (B) prepared from water.

Conclusion

In conclusion, **MTM**-based polyacrylamide copolymers were synthesised and transformed into their corresponding gels after exposing their solutions to UV light (λ = 365 nm). Depending on the crosslink density, these materials exhibited different mechanical and physical properties, which was attributed to the difference in **MTM** content incorporated into the polymer precursors. The 10 and 20% **MTM** were found to be brittle materials while the 5% **MTM** material appeared flexible and highly stretchable. The swelling behaviour demonstrated the inversely proportional relationship between the crosslink density and the amount of water absorbed by the xerogels. The rheological characterisation further evidenced the direct effect of the **MTM** content on the storage and loss moduli in amplitude and frequency sweep experiments. The photo-gels were formulated in both aqueous and

organic solvents, and investigated using SEM, showing the hydrogels of 5 and 10% **MTM** exhibited phase separation, which resulted in the formation of macro-porous materials. On the other hand, the organo-gels did not form any macro-pores and appeared to be well packed. This report introduced the first method of synthesising **MTM**-functional polymers that can be transformed into covalent networks under UV light *via* the [2+2] photocycloaddition of **MTMs**. Although the strategy used to synthesise these scaffolds involves a multi-step process, it provides a broad scope to access different photocurable materials with ranging properties by changing the bromomaleimide N-substituent and/or amine used in the thiolactone ring opening.

SUPPORTING INFORMATION

Additional figures and tables, experimental procedures, instrumentation, synthetic procedures, and supporting characterisation of the synthesised materials.

ACKNOWLEDGMENTS

The authors would like to thank the University of Warwick (M. A., H. A. H., S. E., D. M. H., P. W.) and the University of Taif (M. A.) for financial support. H.A.H. acknowledges funding of his EUTOPIA-SIF fellowship received from the European Union's Horizon 2020 research and innovation programme under the Marie Skłodowska-Curie grant agreement No 945380. The authors acknowledge the use of the University of Warwick polymer characterisation RTP equipment (UV-Vis, FT-IR, GPC, rheology, and mechanical testing) and the Electron Microscopy RTP. P.W. thanks the Royal Society and Tata companies for the award of a University Research Fellowship (URF\R1\180274).

version arising from this submission. Raw data files for the figures presented in the manuscript have been deposited in a local open access repository at Warwick (https://wrap.warwick.ac.uk/) and are also available on request.

KEYWORDS

[2+2] photodimerisation, monothiomaleimides, photocrosslinking, homocysteine thiolactone, polyacrylamide,

References

1. Thiele, J.; Ma, Y.; Bruekers, S. M. C.; Ma, S.; Huck, W. T. S. 25th Anniversary Article: Designer Hydrogels for Cell Cultures: A Materials Selection Guide. *Adv. Mater.* **2014**, *26* (1), 125–148.
2. Vermonden, T.; Censi, R.; Hennink, W. E. Hydrogels for Protein Delivery. *Chem. Rev.* **2012**, *112*, 2853–2888.
3. Mohammed, J. S.; Murphy, W. L. Bioinspired Design of Dynamic Materials. *Adv. Mater.* **2009**, *21*, 2361–2374.
4. Liang, B.; He, X.; Hou, J.; Li, L.; Tang, Z. Membrane Separation in Organic Liquid: Technologies, Achievements, and Opportunities. *Adv. Mater.* **2019**, *31*, 1806090.
5. Du, P.; Wu, M.; Liu, X.; Zheng, Z.; Wang, X.; Joncheray, T.; Zhang, Y. Diels–Alder-Based Crosslinked Self-Healing Polyurethane/Urea from Polymeric Methylene Diphenyl Diisocyanate. *J. Appl. Polym. Sci.* **2014**, *131*, 1-7.
6. Nguyen, L.-T. T.; Truong, T. T.; Nguyen, H. T.; Le, L.; Nguyen, V. Q.; Van Le, T.; Luu, A. T. Healable Shape Memory (Thio)Urethane Thermosets. *Polym. Chem.* **2015**, *6*, 3143–3154.
7. Tan, L.; Quang, H.; Thuy, D.; Phung, T.; Thu, T. Macromolecular Design of a Reversibly Crosslinked Shape-Memory Material with Thermo-Healability. *Polymer,* **2020**, *188*.
8. Rivero, G.; Nguyen, L.-T. T.; Hillewaere, X. K. D.; Du Prez, F. E. One-Pot Thermo-Remendable Shape Memory Polyurethanes. *Macromolecules* **2014**, *47*, 2010–2018.
9. Phelps, E. A.; Enemchukwu, N. O.; Fiore, V. F.; Sy, J. C.; Murthy, N.; Sulchek, T. A.; Barker, T. H.; García, A. J. Maleimide Cross-Linked Bioactive PEG Hydrogel Exhibits Improved Reaction Kinetics and Cross-Linking for Cell Encapsulation and In Situ Delivery. *Adv. Mater.* **2012**, *24*, 64–70.
10. Fu, Y.; Kao, W. J. In Situ Forming Poly(Ethylene Glycol)-Based Hydrogels via Thiol-Maleimide Michael-Type Addition. *J. Biomed. Mater. Res. Part A* **2011**, *98A*, 201–211.
11. Jansen, L. E.; Negrón-Piñeiro, L. J.; Galarza, S.; Peyton, S. R. Control of Thiol-Maleimide Reaction Kinetics in PEG Hydrogel Networks. *Acta Biomater.* **2018**, *70*, 120–128.
12. Guaresti, O.; Basasoro, S.; González, K.; Eceiza, A.; Gabilondo, N. In Situ Cross–linked Chitosan Hydrogels via Michael Addition Reaction Based on Water–soluble Thiol–maleimide Precursors. *Eur. Polym. J.* **2019**, *119*, 376–384.
13. Kuckling, D.; Hoffmann, J.; Plötner, M.; Ferse, D.; Kretschmer, K.; Adler, H.-J. P.; Arndt, K.-F.; Reichelt, R. Photo Cross-Linkable Poly(N-Isopropylacrylamide) Copolymers III: Micro-Fabricated Temperature Responsive Hydrogels. *Polymer.* **2003**, *44*, 4455–4462.
14. Abdelaty, M. S. A.; Kuckling, D. Synthesis and Characterization of New Functional Photo Cross-Linkable Smart Polymers Containing Vanillin Derivatives. *Gels* **2016**, *2*.

15. Abdelaty, M.S.A. Environmental Functional Photo-Cross-Linked Hydrogel Bilayer Thin Films from Vanillin. *J Polym Environ* **2018,** *26*, 2243–2256.
16. Seiffert, S.; Oppermann, W.; Saalwächter, K. Hydrogel Formation by Photocrosslinking of Dimethylmaleimide Functionalized Polyacrylamide. *Polymer.* **2007**, *48*, 5599–5611.
17. Schmeling, N.; Hunger, K.; Engler, G.; Breiten, B.; Rölling, P.; Mixa, A.; Staudt, C.; Kleinermanns, K. Photo-Crosslinking of Poly[Ethene-Stat-(Methacrylic Acid)] Functionalised with Maleimide Side Groups. *Polym. Int.* **2009**, *58*, 720–727.
18. Kamiya, Y.; Takagi, T.; Ooi, H.; Ito, H.; Liang, X.; Asanuma, H. Synthetic Gene Involving Azobenzene-Tethered T7 Promoter for the Photocontrol of Gene Expression by Visible Light. *ACS Synth. Biol.* **2015**, *4*, 365–370.
19. Decker, C.; Bianchi, C. Photocrosslinking of a Maleimide Functionalized Polymethacrylate. *Polym. Int.* **2003**, *52*, 722–732.
20. Harmon, M. E.; Kuckling, D.; Frank, C. W. Photo-Cross-Linkable PNIPAAm Copolymers. 5. Mechanical Properties of Hydrogel Layers. *Langmuir* **2003**, *19*, 10660–10665.
21. Kalaoglu-Altan, O. I.; Sanyal, R.; Sanyal, A. Micropatterned Reactive Nanofibers: Facile Fabrication of a Versatile Biofunctionalizable Interface. *ACS Appl. Polym. Mater.* **2020**, *2*, 4026–4036.
22. Cengiz, N.; Gevrek, T. N.; Sanyal, R.; Sanyal, A. Fabrication of Patterned Hydrogel Interfaces: Exploiting the Maleimide Group as a Dual Purpose Handle for Cross-Linking and Bioconjugation. *Bioconjugate Chem.* **2020**, *31*, 1382-1391.
23. Tsurkan, M. V; Jungnickel, C.; Schlierf, M.; Werner, C. Forbidden Chemistry: Two-Photon Pathway in [2+2] Cycloaddition of Maleimides. *J. Am. Chem. Soc.* **2017**, *139*, 10184–10187.
24. Tedaldi, L. M.; Aliev, A. E.; Baker, J. R. [2 + 2] Photocycloadditions of Thiomaleimides. *Chem. Commun.* **2012**, *48*, 4725–4727.
25. Richards, D. A.; Fletcher, S. A.; Nobles, M.; Kossen, H.; Tedaldi, L.; Chudasama, V.; Tinker, A.; Baker, J. R. Photochemically Re-Bridging Disulfide Bonds and the Discovery of a Thiomaleimide Mediated Photodecarboxylation of C-Terminal Cysteines. *Org. Biomol. Chem.* **2016**, *14*, 455–459.
26. Aljuaid, M.; Liarou, E.; Town, J.; Baker, J. R.; Haddleton, D. M.; Wilson, P. Synthesis and [2+2]-Photodimerisation of Monothiomaleimide Functionalised Linear and Brush-like Polymers. *Chem. Commun.* **2020**, *56*, 9545–9548.
27. Espeel, P.; Du Prez, F. E. One-Pot Multi-Step Reactions Based on Thiolactone Chemistry: A Powerful Synthetic Tool in Polymer Science. *Eur. Polym. J.* **2015**, *62*, 247–272.
28. Reese, C. M.; Thompson, B. J.; Logan, P. K.; Stafford, C. M.; Blanton, M.; Patton, D. L. Sequential and One-Pot Post-Polymerization Modification Reactions of Thiolactone-Containing Polymer Brushes. *Polym. Chem.* **2019**, *10*, 4935–4943.
29. Norioka, C.; Inamoto, Y.; Hajime, C.; Kawamura, A.; Miyata, T. A Universal Method to Easily Design Tough and Stretchable Hydrogels. *NPG Asia Mater.* **2021**, *13*.
30. Canal, T.; Peppas, N. A. Correlation between Mesh Size and Equilibrium Degree of Swelling of Polymeric Networks. *J. Biomed. Mater. Res.* **1989**, *23*, 1183–1193.
31. De France, K. J.; Xu, F.; Hoare, T. Structured Macroporous Hydrogels: Progress, Challenges, and Opportunities. *Adv. Healthc. Mater.* **2018**, *7*, 1700927.
32. Efstathiou, S.; Wemyss, A. M.; Patias, G.; Al-Shok, L.; Grypioti, M.; Coursari, D.; Ma, C.; Atkins, C. J.; Shegiwal, A.; Wan, C.; Haddleton, D. M. Self-Healing and Mechanical Performance of Dynamic Glycol Chitosan Hydrogel Nanocomposites. *J. Mater. Chem. B* **2021**, *9*, 809–823.